

WAVESPACE: A HIGHLY EXPLORABLE WAVETABLE GENERATOR

Hazounne Lee¹

Kihong Kim²

Sungho Lee¹

Kyogu Lee¹

¹ Department of Intelligence and Information, Seoul National University

² Department of Mathematics, Kyungpook National University

{hazounne, sh-lee, kglee}@snu.ac.kr, kimgihong2510@knu.ac.kr

ABSTRACT

Wavetable synthesis generates quasi-periodic waveforms of musical tones by interpolating a list of waveforms called wavetable. As generative models that utilize latent representations offer various methods in waveform generation for musical applications, studies in wavetable generation with invertible architecture have also arisen recently. While they are promising, it is still challenging to generate wavetables with detailed controls in disentangling factors within the latent representation. In response, we present *Wavespace*, a novel framework for wavetable generation that empowers users with enhanced parameter controls. Our model allows users to apply pre-defined conditions to the output wavetables. We employ a variational autoencoder and completely factorize its latent space to different waveform styles. We also condition the generator with auxiliary timbral and morphological descriptors. This way, users can create unique wavetables by independently manipulating each latent subspace and descriptor parameters. Our framework is efficient enough for practical use; we prototyped an oscillator plug-in as a proof of concept for real-time integration of *Wavespace* within digital audio workspaces (DAWs).

1. INTRODUCTION

Among many real-time synthesis methods of musical tones, wavetable synthesis has been widely used to generate quasi-periodic waveforms [1]. Wavetable synthesis retrieves single-cycle waveforms from a wavetable. Compared to other sound synthesis techniques, this method empowers users to create more general or evolving waveforms by interpolation of waveforms with efficient memory usage [2]. While the previous restriction of computation and memory usage is highly mitigated, it is still recognizably used in applications for musical tone synthesis with a wide range of sound textures [3, 4].

Meanwhile, researchers have studied waveform generation with deep neural networks [5, 6]. One of the widely-used methods utilizes audio latent representation in autoencoder structure [7, 8], especially for musical tone genera-

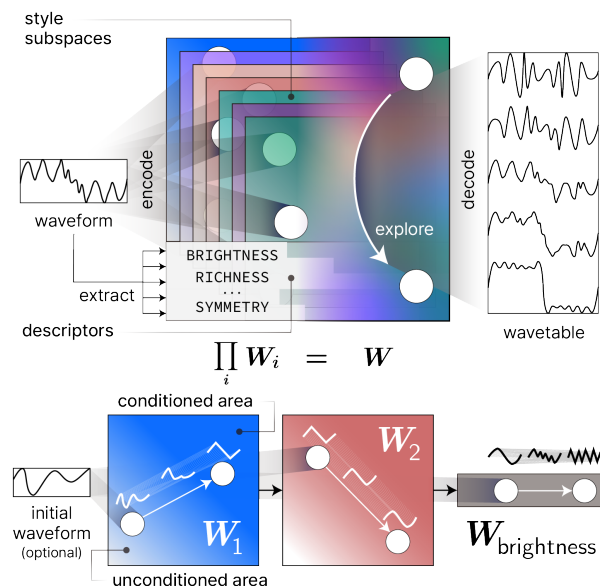


Figure 1: The *Wavespace* framework enables waveform creation through subspace encoding and interpolation. Each subspace latent is adjustable independently.

tion [9–12]. Research on waveform generation for musical applications with these architectures has been emerging in the last few years [12–16]. One of the applications is the neural wavetable generator, which synthesizes a series of single-cycle waveforms from the latent space to construct a wavetable [17, 18]. Wavetables can be generated by interpolation of latent vectors, enabling distinctive non-linear blending between waveforms [19]. This commonly utilizes generative models such as variational autoencoders (VAEs). More recently, studies have used this autoencoder structure for an oscillator with real-time waveform generation. By decoding a waveform for every audio buffer request, the latent space replaces the functionality of the wavetable. This method is a novel way of generating quasi-periodic waveforms because the latent space exploration allows obtaining various waveforms with smooth transitions between them [20]. It has a similar concept to vector synthesis in the aspect of exploring a given space to generate real-time single-cycle waveforms [21]. This approach is more general than generating wavetables but is also challenging because of the computation speed restriction. In short, current studies focus on either wavetable generation or oscillator implementation. They aim to enable users to

arXiv:2407.19862v1 [cs.LG] 29 Jul 2024



generate waveforms utilizing latent representations. However, it is challenging for users to select specific waveform styles since the latent space is entangled.

To reduce this gap, we present `Wavespace`, a highly explorable wavetable generator with complete conditional controls. Figure 1 represents `Wavespace` and its instructions for wavetable generation. Compared to the previous methods, `Wavespace` explicitly factorizes its latent space so that each subspace modifies the style of the waveform in a more interpretable manner. This way, users can understand how each latent space parameter works. Specifically, we disentangle the latent space into style subspaces. Waveforms are encoded to each style subspace, and auxiliary descriptors are algorithmically extracted. Users can control the style and descriptor parameters to obtain wavetables from scratch. First, they initialize the parameters by exploring the latent space. Encoding a waveform and extracting descriptors can be another way to do it. They can adjust the parameters to transform the waveform. For example, in the style subspace W_1 the output waveform morphs to the corresponding style by moving the parameter from the unconditioned area to the conditioned area. General waveforms with subtle changes are obtained by passing through two areas as seen in the style subspace W_2 . Increasing the parameter in descriptor $W_{\text{brightness}}$ adds more brightness to the waveform. These parameter manipulations accompany a smooth transition in the waveform. Our model is based on conditional variational autoencoder (CVAE) [22] structure. The latent space is variationally trained with algorithmically extracted descriptors concatenated. With `Wavespace` and its plug-in implementation, our major contributions are as follows:

- We introduce `Wavespace`, a novel framework for flexible and controllable wavetable generation from factorized latent space.
- We propose a method encompassing wavetable generation and a real-time autoencoder-based oscillator with complete conditional controls.
- We build an audio plug-in based on `Wavespace` with a user interface and show its real-time use in the CPU.

2. BACKGROUND

2.1 Wavetable Synthesis

Wavetable synthesis employs fixed-size single-cycle waveforms $x_1, \dots, x_M \in \mathbb{R}^N$ where M and N denote the number of waveforms and their length in samples, respectively. We stack these waveforms to form a so-called ‘‘wavetable’’ $\mathbf{X} \in \mathbb{R}^{M \times N}$. Then, we can generate a signal $s[n]$ from the wavetable \mathbf{X} with a read operation Φ given as follows,

$$s[n] = \Phi(\mathbf{X}, \tilde{i}[n], \tilde{j}[n]) \quad (1)$$

where $\tilde{i}[n]$ and $\tilde{j}[n]$ are row and column indices, respectively. The row index $\tilde{i}[n]$ selects the waveform to use. It is typically a time-varying signal, which changes or ‘‘morphs’’ the shape of waveform across time. The column

indices $\tilde{j}[n]$ are determined by the time-varying (instantaneous) fundamental frequency $f_0[n]$ and given as follows,

$$\tilde{j}[n] = \left\lfloor \frac{N}{f_s} \sum_{m=0}^n f_0(m) \right\rfloor \% N. \quad (2)$$

where f_s and $\%$ denote a sampling rate and modulo operation, respectively. When both indices are integers, we can obtain the desired sample by reading the table element: $s[n] = \mathbf{X}[\tilde{i}[n], \tilde{j}[n]]$. Otherwise, the read operation Φ interpolates the nearest samples in the wavetable \mathbf{X} , e.g., in a (bi-)linear manner.

2.2 Neural Wavetable Generators

Instead of relying on a fixed and pre-defined wavetable \mathbf{X} , existing works employ an autoencoder framework, using a pair of encoder \mathcal{E} and decoder \mathcal{D} to obtain a generative model of single-cycle waveforms. Once trained, one can obtain a novel wavetable \mathbf{X} by decoding a series of latent vectors $\mathbf{w}_1, \dots, \mathbf{w}_M \in W$ as follows,

$$\mathbf{X} = [x_1, \dots, x_M] = [\mathcal{D}(\mathbf{w}_1), \dots, \mathcal{D}(\mathbf{w}_M)]. \quad (3)$$

[19] shows the basic concept of the neural wavetable generator. The authors demonstrate blending two single-cycle waveforms by latent interpolation, allowing for the creation of intermediate waveforms. However, the method’s reliance on a large model hinders real-time generation.

There are studies for wavetable generators focusing on real-time autoencoder-based oscillators. [20] introduce this oscillator concept with VAE architecture. While its method allows for generating various waveforms with smooth transitions, the entangled latent space makes it difficult and time-consuming for users to navigate and find the specific sounds they desire. [18] present a method for generating single-cycle waveforms using timbral descriptors. However, this approach requires an input waveform to be morphed, limiting its ability to create waveforms from scratch. The latent space entanglement is the direct cause of this limitation. We factorize the latent space and integrate the separate wavetable generation methods into `Wavespace` framework with sufficient parameters to craft waveforms.

3. METHOD

We build upon the architecture of our baseline described in [18]. The baseline model has a CVAE structure with both time-domain input and output, employing three timbral descriptors. It consists of 1D convolutional and transposed convolutional layers.

3.1 Learning Latent Subspaces

The parameter space W is a product of the style latent space W_S and the descriptor space W_D . S and D refer to a set of styles and descriptors. We can break down the parameter space as follows:

$$W = W_S \times W_D = \prod_{s \in S} W_s \times \prod_{d \in D} W_d \quad (4)$$

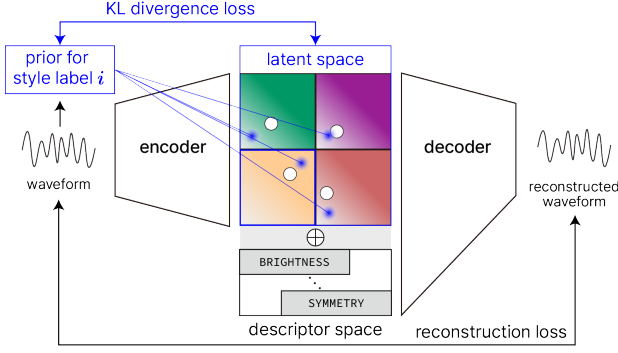


Figure 2: Our model’s training method learns latent subspaces. Priors depend on the target style label. The prior within the blue-bordered subspace has a unique position.

We learn latent subspaces $W_s (s \in S)$ to factorize the latent space, inspired by [23]. The study replaces condition concatenation with another variationally trainable latent space. \mathbf{s} and \mathbf{d} are style and descriptor parameters. For $\mathbf{s}_j \in W_j$, the prior in j th latent subspace, $p_i(\mathbf{s}_j)$, differs from two situations; the label corresponds to the subspace ($i = j$) or otherwise ($i \neq j$). The subspace prior switches as

$$p_i(\mathbf{s}_j) \sim \begin{cases} \mathcal{N}(\mu_{0j}, \sigma_{0j}^2), & i \neq j \\ \mathcal{N}(\mu_{1j}, \sigma_{1j}^2), & i = j \end{cases}, \quad (5)$$

for $i, j = 0, 1, 2, \dots, N - 1$. μ_{0j} , μ_{1j} , σ_{0j}^2 , and σ_{1j}^2 , which are the mean and variance of Gaussian distribution. Note that only the i th subspace has a different subspace prior, i.e. $p_i(\mathbf{s}_i)$. We had experiments μ_{0j} and μ_{1j} both fixed and learned from random initialization. A joint prior for target i is obtained as

$$p_i(\mathbf{s}) = \prod_{j=0}^{N-1} p_i(\mathbf{s}_j) \sim \mathcal{N}(\mu_i, \sigma_i^2). \quad (6)$$

The assumption on this statement is that $p_i(\mathbf{s}_j)$ is mutually independent for every j . This method disentangles the style subspaces and integrates them into a shared latent space. Then, we optimize the variational evidence lower bound as an objective given as follows,

$$\mathbb{E}_{q_\phi(\mathbf{s}|\mathbf{x}, \mathbf{d})} [\log p_\theta(\mathbf{x}|\mathbf{s}, \mathbf{d})] - D_{\text{KL}}(q_\phi(\mathbf{s}|\mathbf{x}, \mathbf{d}) || p_i(\mathbf{s})). \quad (7)$$

This loss aims to generate waveforms according to the style latent space parameters, by learning properly both $q_\phi(\mathbf{s}|\mathbf{x}, \mathbf{d})$ and $p_\theta(\mathbf{x}|\mathbf{s}, \mathbf{d})$. The overall scheme of learning latent subspaces is illustrated in Figure 2.

3.2 Descriptor Extraction

We obtain timbral descriptors from relevant spectral audio features based on the method utilized in [18, 24]. Readers can refer to [25] and references therein for the relation between audio features and timbral descriptors. Moreover, we add morphological descriptors which are obtained from waveform features. Although these features may not be independent of the timbre, they allow particular morphs in

sound texture in distinctive ways. For some descriptors, we extract features and then compress their range with the following function σ defined as follows,

$$\sigma(d) = \frac{\log(d \times (e^k - 1) + 1)}{k} \quad (8)$$

where the hyperparameter k is empirically set to 5.5. Below are the details of the descriptors.

- **Brightness** — The spectral centroid refers to the center of mass of the spectrum indicating the balance between low and high-frequency energy. We relate the brightness of the sound to the spectral centroid as

$$d_B(x) = \sigma \left(\sum_{k=0}^{N/2} k |X[k]|^2 \right) \quad (9)$$

where X denotes the discrete Fourier transform (DFT) of the single-cycle waveform x .

- **Richness** — Similar to brightness, we relate harmonic spread to the richness of the sound.

$$d_R(x) = \sigma \left(\sum_{k=0}^{N/2} |(k - C)X[k]|^2 \right) \quad (10)$$

where C is the spectral centroid defined as above but before the compression σ .

- **Fullness** — This feature is opposite to the warmth, which is discovered from sounds without even overtones. Thus, we use the power ratio between the odd overtones and the total overtones.

$$d_F(x) = 1 - \frac{\sum_{k=0}^{N/4-1} |X[2k+1]|^2}{\sum_{k=0}^{N/2} |X[k]|^2}. \quad (11)$$

- **Undulation** — We assume that the difference of a signal is employable for distinctive timbral manipulation. We use the scaled absolute of difference to quantify the “zigzagness” of a waveform.

$$d_U(x) = \frac{1}{N-1} \cdot \sigma \left(\sum_{n=0}^{N-2} |x[n+1] - x[n]| \right). \quad (12)$$

- **Symmetry** — We employ the angle of the sum of all the magnitude components to improve the model to distinguish between two waveforms that have the same amplitude but different phases.

$$d_S(x) = \angle \left(\sum_{k=0}^{N/2} X[k] \right). \quad (13)$$

Our hypothesis is that concatenating these descriptors would improve the quality of reconstruction and latent representation. This is because we provide additional information about the waveform in various ways, which may not be captured from the low-dimensional subspaces.

3.3 Architecture Details

The encoder consists of six 1D convolution blocks, each including Leaky ReLU of negative slope of 0.2 and batch normalization, followed by the final linear layer and reparametrization, outputting values for style latent space. Descriptors are concatenated to the latent space and then passed to the decoder. The decoder comprises 6 blocks of upsampling and residual layers, in which a Transposed 1D convolution and three 1D convolution layers are used, respectively. The decoder outputs raw waveform. The final waveform is normalized to the power of 1 with any constant offset eliminated.

4. EXPERIMENTS

4.1 Datasets

According to [20], the model capacity relies heavily on the dataset used for training. To evaluate the model performance with different datasets we utilize two different datasets. We train our baseline architecture with our dataset and compare it to our model.

- **Serum** — We conduct experiments using wavetables extracted from the Serum VST plugin, a widely recognized standard in the field of wavetable synthesizers¹. We select 18 wavetables and assign them to each style. Each wavetable has 256 waveforms of 2048 samples.
- **WaveEdit** — we use open-source wavetables provided on WaveEdit Online². We divide the dataset into two styles randomly. Each wavetable has 2572 waveforms of 256 samples.

We preprocess the waveforms as follows. First, we resample them to model input size, which is 1024 and 600 for our models and the baseline respectively. We also eliminate any constant offset. Then, the total energy of the waveform is normalized to 1. To reduce the variance of the experimental results, we employ 5-fold cross-validation and report the average results.

4.2 Model

We use two versions of our model: WS (~1.7M) and WS-S (~111K parameters), where “S” denotes “small”. Priors are set to $\mu_{0i} = (0, 0)$, $\mu_{1i} = (5, 5)$, and $\sigma_{0i} = \sigma_{1i} = 1$ for every i . We conduct additional experiments of learning μ_i in priors. In this case, each μ_i is set in hyperspherical coordinates and learns angles to keep $|\mu_i| = 5$. We use 2-dimensional style subspaces.

4.3 Optimization

We draw upon (7) to construct the total loss. The total loss is formulated as

$$\mathcal{L} = \beta_1 \mathcal{L}_s + \beta_2 D_{\text{KL}}(q_\phi(\mathbf{w}|\mathbf{x}, \mathbf{y})||p_i(\mathbf{w})) + \beta_3 \mathcal{L}_w. \quad (14)$$

¹<https://xferrecords.com/products/serum/>

²<https://waveeditonline.com/>

Here, \mathcal{L}_s and \mathcal{L}_w are the spectral loss and waveform loss respectively. \mathcal{L}_w is an L_1 norm loss for learning the waveform shape, and \mathcal{L}_s is an L_2 norm loss of spectral amplitude. The first two terms are related to (7) for learning the spectral representation and the encoder distribution. Because we use Gaussian priors, the reconstruction term $-\mathbb{E}_{q_\phi(\mathbf{s}|\mathbf{x}, \mathbf{d})} [\log p_\theta(\mathbf{x}|\mathbf{s}, \mathbf{d})]$ requires to be an L_2 norm loss. Therefore, we first assign L_s to this term and introduce additional waveform loss L_w . Each loss term is weighted by the corresponding coefficients and then summed up.

We found that a large β_3 in the early training stage helps the model effectively learn the waveform shape. Hence, we use an exponentially decreasing schedule for its weight β_w as follows,

$$\beta_3(\text{epoch}) = \beta_3^{(0)} \times (20 \exp(-r \times \text{epoch}) + 1) \quad (15)$$

where the decrease rate r is 0.144.

We empirically set the weights of the loss terms to $\beta_1 = 0.354$, $\beta_2 = 2.231$, and $\beta_3^{(0)} = 4.170$. We use a LinearLR learning rate scheduler in Pytorch [26] with `start_factor` of 1.0, `end_factor` of 0.5, and `total_iters` of 1500. We train the model for a total of 5000 epochs.

5. RESULTS

Our model is evaluated for its capacity and computational efficiency in wavetable generation. If not specified, the evaluation is conducted using the test dataset from Serum and our WS model.

5.1 Wavetable Generation

We demonstrate wavetable generation by adjusting parameters in style subspaces and descriptors. We conduct wavetable generation by the latent space interpolation across two styles. We select two different wavetables that represent each style. We excerpt 5 waveforms at equal intervals and pair them sharing the same wavetable position. We encode them with extracted descriptors and linearly interpolate between the paired parameters in the latent space. Figure 3 shows the wavetable generation between two wavetables in different styles. We conclude that the smooth transition between two waveforms of different styles allows us to generate wavetables of unseen waveforms that include novel sonic textures. We also show how each descriptor parameter morphs the waveform in Figure 4. The waveforms morph distinctively according to the given descriptor. Notably, our proposed morphological descriptors work along our assumption.

5.2 Generation Capacity

5.2.1 Latent Space Factorization

Figure 5 shows the distribution of our data and latent representations. Our model effectively disentangles waveform styles as KL divergence indicated to 0.133, which is lower than 0.393 of the baseline. Hence, the encoder

Table 1: Comparison of generation capacity including reconstruction and descriptor errors in Serum and WaveEdit(WE) datasets. Small models and prior learning are indicated in S and PL. Each metric is the average of elements.

Model	Waveform MAE		Spectral MSE		Descriptor MAE									
	Serum	WE	Serum	WE	Brightness		Richness		Fullness		Undulation		Symmetry	
					Serum	WE	Serum	WE	Serum	WE	Serum	WE	Serum	WE
Baseline	0.054	0.055	0.177	0.488	0.047	0.080	0.045	0.045	0.070	0.121	–	–	–	–
WS	0.005	0.035	0.018	0.221	0.026	0.068	0.103	0.189	0.019	0.161	0.015	0.046	0.183	0.730
WS-S	0.008	0.038	0.033	0.240	0.062	0.097	0.204	0.239	0.033	0.231	0.029	0.055	0.376	0.926
WS-PL	0.017	0.038	0.117	0.250	0.050	0.074	0.126	0.203	0.079	0.185	0.026	0.049	0.454	0.811
WS-S-PL	0.024	0.045	0.170	0.309	0.092	0.105	0.213	0.240	0.136	0.311	0.041	0.058	0.791	1.067

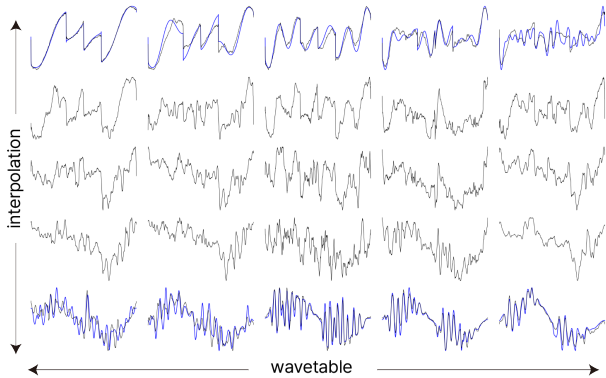


Figure 3: Latent space interpolation between two styles. Black and blue waveforms are the generated ones and the ground truth, respectively.

distinguishes the waveform styles better than the previous method. However, our prior learning model shows 25.133 to this metric, indicating the encoder’s low performance. As we found that the learning priors are not converging to certain values, we suggest that they hinder learning latent subspaces because the criteria for calculating KL divergence keep changing, leading to unstable training. We also take the analysis of the feedback latents by feeding back reconstructed waveforms into the encoder. The t-SNE plot indicates clear disentanglement of the feedback latents. The KL divergence for feedback latents is 0.116, which is lower than the original latent representation. This demonstrates the decoder’s capability to generate waveforms according to a style.

5.2.2 Reconstruction

We evaluate our model with mean absolute error (MAE) between the waveform domain and mean square error (MSE) in the magnitude spectrum domain. We calculate descriptor errors by MAE between extracted descriptors from \hat{x} and x . The MAE of symmetry $\text{Sym}(\hat{x}, x)$ passes an additional operation

$$\text{Sym}'(\hat{x}, x) = -|(\text{Sym}(\hat{x}, x) \bmod 2\pi) - \pi| + \pi \quad (16)$$

to avoid a loss bigger than π since we only measure the smaller angle. Table 1 indicates the reconstruction capacity of the baseline and our models. Our proposed model shows exceptional outperforming in waveform MAE and

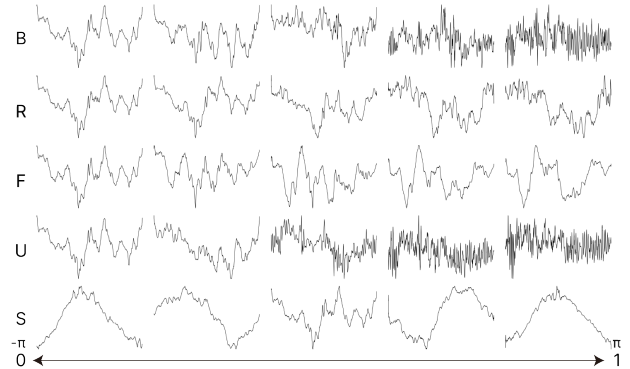


Figure 4: Effect of the descriptors. We gradually adjust each descriptor in 5 steps between 0.2 to 1.0 ($-\pi$ to π for symmetry), fixing style latents at zero.

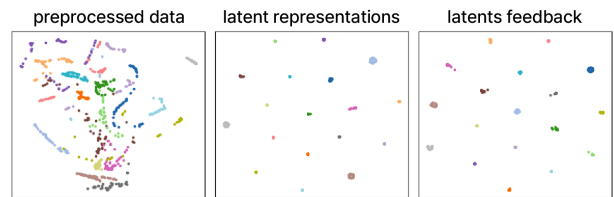


Figure 5: t-SNE scatter plot of preprocessed test data, the latents, and the feedback latents. Different colors represent different wavetables.

spectral MSE compared to the baseline. Our models are also competent capacity in the descriptor MAE, especially in brightness. Our models with learnable priors indicate the minimum reconstruction performance. We conclude that training the priors is not the best choice for learning latent subspace. Comparing the results between the two datasets, it is clear that the performance generally excels in the Serum dataset. Thus, reconstruction capacity highly depends on the training dataset, which is analogous to the results in [24].

5.3 Ablation Study

We provide more information about the various settings we have tested, indicating the relationship between our methods and reconstruction capacity. We discuss three elements of our experiment; see Table 2. First, we can get rid of the use of descriptors and the relative losses (① in Table 2).

Table 2: Ablation study results (Serum dataset). The original model’s performance is shown in the top row. Descriptors are indicated in their initials.

①	②	③	MAE	MSE	B	R	F	U	S
✓	✗	✗	0.005	0.018	0.026	0.103	0.019	0.015	0.183
✗	✗	✗	0.015	0.086	0.083	0.140	0.126	0.033	0.468
✗	✗	✓	0.022	0.147	0.116	0.171	0.178	0.047	0.686
✓	✓	✗	0.005	0.023	0.064	0.143	0.020	0.019	0.077
✓	✗	✓	0.012	0.037	0.040	0.112	0.054	0.022	0.490
✓	✓	✓	0.012	0.041	0.055	0.097	0.049	0.019	0.097

① Descriptors ② Descriptor Loss ③ Spectral Output

Table 3: The decoders’ computational efficiency in CPU. Time refers to the generation time per waveform.

Model	# of Params	FLOPs ($\times 10^6$)	Computation Speed	
			Time (ms)	RTF
Baseline	1.2M	66.902	26.2	0.81
WS	1.2M	3.443	17.2	1.24
WS-S	76.3K	0.219	9.7	2.20

Second, we add L_1 descriptor loss with coefficients $\beta_4 \cdot \mathcal{L}_d$, where $\beta_4 = [4.17, 4.17, 4.17, 10, 40]$. We calculate descriptor loss using the same method as the evaluation metrics (② in Table 2). Lastly, we change the direct waveform output to the spectral components. The spectral components consist of magnitude $|X|$ and phase $\angle X$ where X denotes the DFT of the single waveform x . We convert back to the time domain via inverse Fast Fourier Transform (③ in Table 3). We train models with altered settings and evaluate their reconstruction capacity. The results show that our current setup has overall better reconstruction quality than the other alternatives.

5.4 Computational Efficiency

To use *Wavespace* in real-time audio plug-ins, it is crucial to check whether the decoder’s computational efficiency is within the appropriate generation speed. We report floating-point operations (FLOPs) and real-time factor (RTF) for averaged 100 times of dataset in Table 3. We calculate the RTF as processing time divided by buffer duration. Assuming that we choose 1024 buffer length with a 48000Hz sample rate, the buffer duration is approximately 21.3 milliseconds. We utilize the M1 CPU chip of the 2020 version MacBook. Therefore, our proposed model’s decoder performs real-time generation under typical buffer duration settings.

6. PLUG-IN IMPLEMENTATION

We have proved that our model’s RTF quantitatively grants real-time capacity. As a proof of concept for real-time use, we prototype an autoencoder oscillator that leverages our *Wavespace*. When implementing a real-time virtual instrument with the pre-trained model, finding an appropri-

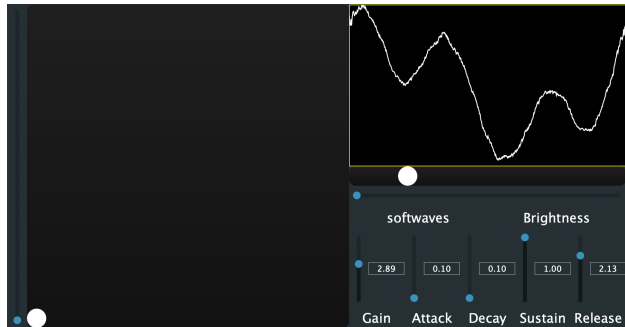


Figure 6: The snapshot of our VST plug-in implemented based on *Wavespace*.

ate policy for requesting every new waveform is crucial. To make it stable under buffer constraints, we (i) execute the model only when parameters change and (ii) restrict the maximum frequency of the model executions. We represent the user interface of our plugin in Figure 6. The left rectangle shows a style subspace W_i , and we can switch it to another one using the attached slider. Users can select a point w_i in each subspace W_i . On the right is a visualization of the waveform x_i ; it has a small slider for selecting a timbral or morphological descriptor and a large slider for adjusting its value. Finally, as a basic functionality, we add a gain fader and amplitude envelope with attack, decay, sustain, and release sliders (bottom right). Our plugin is implemented in virtual studio technology (VST) and audio unit (AU) format and will be available online.

7. CONCLUSION

Our study introduced *Wavespace*, a wavetable generator framework with factorized latent space, allowing users to generate wavetables from scratch. By learning latent subspaces in the CVAE structure, our model efficiently generated waveforms corresponding to the given styles and descriptors. We achieved improved reconstruction quality in both waveform and spectral domains. Our model is also computationally efficient, enabling the implementation of a real-time autoencoder-based oscillator.

A crucial question for future work is to identify which factors within the dataset significantly contribute to the model’s generation capacity. Also, future research should investigate methods for combining parameters in a user-friendly manner, allowing users to leverage their control over wavetable generation efficiently. We hope for further discussions on wavetable generation methods and their creative implementation to audio plug-ins.

8. ETHICS STATEMENT

We used wavetables in the Serum, a commercial wavetable synthesizer provided by Xfer Records. The company informed us that there are no legal guidances for the license using Serum wavetables beyond music making and sound design. Thus, we did our best to prevent any damage our research may cause to Xfer Records in terms of usage. Our

research never shares with anyone (i) any implementation of Serum and (ii) raw wavetable datasets from Serum.

9. REFERENCES

- [1] R. Bristow-Johnson, “Wavetable synthesis 101, a fundamental perspective,” in *Audio engineering society convention 101*. Audio Engineering Society, 1996.
- [2] A. Franck and V. Välimäki, “Higher-order integrated wavetable synthesis,” in *Proceedings of the International Conference on Digital Audio Effects (DAFx)*, York, UK, 2012, pp. 17–21.
- [3] A. Horner, “A comparison of wavetable and fm parameter spaces,” *Computer Music Journal*, vol. 21, no. 4, pp. 55–85, 1997.
- [4] R. C. Maher, “Wavetable synthesis strategies for mobile devices,” *Journal of the Audio Engineering Society*, vol. 53, no. 3, pp. 205–212, 2005.
- [5] A. v. d. Oord, S. Dieleman, H. Zen, K. Simonyan, O. Vinyals, A. Graves, N. Kalchbrenner, A. Senior, and K. Kavukcuoglu, “Wavenet: A generative model for raw audio,” *arXiv preprint arXiv:1609.03499*, 2016.
- [6] N. Chen, Y. Zhang, H. Zen, R. J. Weiss, M. Norouzi, and W. Chan, “Wavegrad: Estimating gradients for waveform generation,” *arXiv preprint arXiv:2009.00713*, 2020.
- [7] M. Morrison, R. Kumar, K. Kumar, P. Seetharaman, A. Courville, and Y. Bengio, “Chunked autoregressive gan for conditional waveform synthesis,” *arXiv preprint arXiv:2110.10139*, 2021.
- [8] R. Yamamoto, E. Song, and J.-M. Kim, “Parallel wavegan: A fast waveform generation model based on generative adversarial networks with multi-resolution spectrogram,” in *ICASSP 2020-2020 IEEE International Conference on Acoustics, Speech and Signal Processing (ICASSP)*. IEEE, 2020, pp. 6199–6203.
- [9] J. Engel, C. Resnick, A. Roberts, S. Dieleman, M. Norouzi, D. Eck, and K. Simonyan, “Neural audio synthesis of musical notes with wavenet autoencoders,” in *International Conference on Machine Learning*. PMLR, 2017, pp. 1068–1077.
- [10] K. Tatar, D. Bisig, and P. Pasquier, “Latent timbre synthesis: Audio-based variational auto-encoders for music composition and sound design applications,” *Neural Computing and Applications*, vol. 33, pp. 67–84, 2021.
- [11] P. Esling, A. Chemla-Romeu-Santos, and A. Bitton, “Bridging audio analysis, perception and synthesis with perceptually-regularized variational timbre spaces.” in *ISMIR*, 2018, pp. 175–181.
- [12] K. Tahiroğlu, M. Kastemaa, and O. Koli, “Ganspacesynth: A hybrid generative adversarial network architecture for organising the latent space using a dimensionality reduction for real-time audio synthesis,” in *Conference on AI Music Creativity*, 2021.
- [13] J. Engel, L. Hantrakul, C. Gu, and A. Roberts, “Ddsp: Differentiable digital signal processing,” *arXiv preprint arXiv:2001.04643*, 2020.
- [14] J. Hyrkas, “Wavaetable synthesis,” in *International Symposium on Computer Music Multidisciplinary Research*. Springer, 2021, pp. 26–31.
- [15] A. Caillon, A. Bitton, B. Gatinet, and P. Esling, “Timbre latent space: exploration and creative aspects,” *arXiv preprint arXiv:2008.01370*, 2020.
- [16] A. Caillon and P. Esling, “Rave: A variational autoencoder for fast and high-quality neural audio synthesis,” *arXiv preprint arXiv:2111.05011*, 2021.
- [17] D. Högberg, “Latent vector synthesis,” 2023.
- [18] Y. Tsugumasa, “Semantic timbre control of wavetable synthesis using cvae,” University of Tsukuba, Tech. Rep. 2023-MUS-137(8), 2023.
- [19] L. Hantrakul and L.-C. Yang, “Neural wavetable: a playable wavetable synthesizer using neural networks,” *arXiv preprint arXiv:1811.05550*, 2018.
- [20] G. Kreković, “A concept of a wavetable oscillator based on a neural autoencoder,” in *Proceedings of the 16th International Audio Mostly Conference*, 2021, pp. 240–243.
- [21] A. Keating and A. Sklar, “Survey of digital synthesis techniques.”
- [22] K. Sohn, H. Lee, and X. Yan, “Learning structured output representation using deep conditional generative models,” *Advances in neural information processing systems*, vol. 28, 2015.
- [23] J. Klys, J. Snell, and R. Zemel, “Learning latent subspaces in variational autoencoders,” *Advances in neural information processing systems*, vol. 31, 2018.
- [24] G. Kreković, “Deep convolutional oscillator: Synthesizing waveforms from timbral descriptors,” 2022.
- [25] G. Kreković, A. Pošćić, and D. Petrinović, “An algorithm for controlling arbitrary sound synthesizers using adjectives,” *Journal of New Music Research*, vol. 45, no. 4, pp. 375–390, 2016.
- [26] A. Paszke, S. Gross, F. Massa, A. Lerer, J. Bradbury, G. Chanan, T. Killeen, Z. Lin, N. Gimelshein, L. Antiga *et al.*, “Pytorch: An imperative style, high-performance deep learning library,” *Advances in neural information processing systems*, vol. 32, 2019.